Check for updates

JGR Space Physics

RESEARCH ARTICLE
10.1029/2022JA031049

Long-Term Trends in the Upper Atmosphere Using the Incoherent Scatter Radar Observations Over Arecibo

D. Selvaraj[1], Michael P. Sulzer[1], Shun-Rong Zhang[2], and Christiano G. M. Brum[1]

[1]Arecibo Observatory, University of Central Florida (UCF), Arecibo, PR, USA, [2]Haystack Observatory, Massachusetts Institute of Technology, Westford, MA, USA

Key Points:

- Long-term trends of ion temperature at Arecibo show the upper atmosphere is cooling
- Ion temperature cooling trends at Arecibo are significantly larger than the anticipated effects of the global greenhouse gas (GHG) increase
- Nighttime cooling trends in the altitude of ~320–400 km might be caused by the GHG and magnetic field variations

Correspondence to:

D. Selvaraj,
selvarajnkl85@gmail.com;
selvaraj@naic.edu

Citation:

Selvaraj, D., Sulzer, M. P., Zhang, S.-R., & Brum, C. G. M. (2023). Long-term trends in the upper atmosphere using the incoherent scatter radar observations over Arecibo. *Journal of Geophysical Research: Space Physics*, *128*, e2022JA031049. https://doi.org/10.1029/2022JA031049

Received 14 OCT 2022
Accepted 1 FEB 2023

©2023. The Authors.
This is an open access article under the terms of the Creative Commons Attribution License, which permits use, distribution and reproduction in any medium, provided the original work is properly cited.

Abstract Upper atmospheric long-term trends have been characterized through the analysis of the ionospheric ion temperature (T_i). Previous studies used T_i observations from various incoherent scatter radar (ISR) facilities located at different latitudes. In this paper, we analyze Arecibo Observatory's (AO) ISR (18°20'N, 66°45'W) data sets from 1985 to 2019 to detect T_i long-term trends as a function of altitude from ~140 to ~677 km. We empirically modeled the responses of T_i to the known forcings of solar activity, geomagnetic activity, and the annual and semi-annual oscillations. The T_i trend is determined through least squares fitting to the residuals of the T_i, which were estimated by removing the empirically modeled T_i from the observed T_i. Since the ions and neutrals are closely coupled, our results indicate that the upper atmosphere/ionosphere over Arecibo has been cooling over the 35 years studied. Above 350 km, a latitudinal dependency is seen by comparison of all ISR estimated T_i trends, which agrees with the earlier reported results. These observed cooling trends exceed the magnitude expected by the modeling studies from increased greenhouse gas (GHG) concentrations. These excess coolings are as high as −1.2 K/year below 320 km altitude, where an increase in GHG dominates. Nighttime cooling trends in the altitude of ~320–400 km might be caused by the increasing GHG concentrations and magnetic field variations since the trends of AO-ISR match with the Whole Atmosphere Community Climate Model eXtension simulations.

1. Introduction

The increasing concentration of anthropogenic greenhouse gases (GHGs) leads to global warming in the lower atmosphere but can cool the upper atmosphere (Laštovička, 2015, 2021; Laštovička et al., 2006; Roble & Dickinson, 1989). However, the observed upper atmospheric cooling could also be caused by long-term changes in geomagnetic activity (Liu et al., 2021; Mikhailov, 2006), secular changes in the Earth's magnetic field (Cnossen, 2014, 2020a; Qian et al., 2021; Yue et al., 2018), increased gravity wave activity (Oliver et al., 2013), and also other drivers which are in debate (Laštovička, 2015; Oliver et al., 2014, 2015, 2013).

Studies of long-term changes in the upper atmosphere/ionosphere have started after the modeling work of Roble and Dickinson (1989). They found the cooling trends and density decrease in the mesosphere and thermosphere by doubling the CO_2 and CH_4 concentrations in the mesosphere. Also, they found lowered E- and F- layer peak densities. Calculations by Rishbeth (1990) also predicted a decrease in thermospheric density (and therefore the satellite drag) in response to an increase in the concentration of GHGs. Emmert et al. (2004) performed an observational study on the long-term changes of neutral densities using the near-Earth space objects of 1996–2001 at the height around 400 km. There have been various studies of long-term changes in thermosphere density based on observations of satellite drag (Cai et al., 2019; Emmert, 2015; Emmert et al., 2010, 2004, 2008; Keating et al., 2000). The density decreases were in the range of −2% to −5% per decade, about twice as large as predicted by the theory of Roble and Dickinson (1989) (Emmert et al., 2004). These decreasing trends in densities were also found when the effect of solar cycle variability was minimized by evaluating only the solar minimum years (Emmert et al., 2010).

Lowering of the peak height of the F2-layer (hmF2) was found in ionospheric long-term trend studies possibly due to the thermospheric cooling (Bremer, 1992; Brum et al., 2011; Santos et al., 2011). This lowering of peak height could also be associated with the changes in the meridional neutral wind component that became more poleward as reported by Brum et al. (2012). In thermosphere, the meridional wind and F2 parameters are coupled with the ion flow through ion-neutral collisions, playing a direct role in the transport of ionospheric plasma along the magnetic field lines and modifying the ion densities above about 200 km by affecting the rate

21699402, 2023, 2, Downloaded from https://agupubs.onlinelibrary.wiley.com/doi/10.1029/2022JA031049, Wiley Online Library on [02/04/2023]. See the Terms and Conditions (https://onlinelibrary.wiley.com/terms-and-conditions) on Wiley Online Library for rules of use; OA articles are governed by the applicable Creative Commons License

at which the O^+ ions diffuse downward (Santos et al., 2011). Therefore, the lowering of hmF2 caused by the meridional wind found over Arecibo by Brum et al. (2012) and Santos et al. (2011), respectively, agree with the theory, and a decrease in electron density would be expected. However, Santos et al. (2011) have shown that for the same period of 30 years of study despite the lowering of hmF2 at the rate of about 600 m per year, the F2 peak frequency increased/decreased ∼0.015 MHz per year at dusk/dawn periods, showing that the long-term trend changes are somehow a mixture of different factors with different impacts in the thermospheric altitudes yet to be understood. For instance, Holt and Zhang (2008) pointed out some disadvantages in using the F2 peak parameters for inferring the trends of neutral temperature because of the different forcings that modulates it, like the aforementioned meridional wind, composition, and, long-term trends in solar and geomagnetic activity, and secular variations of geomagnetic field orientation. Holt and Zhang (2008) stated that the ion temperature (T_i) is a good representative of neutral temperature up to the height of 400 km, where there exists a close coupling between neutrals and ion components (Holt & Zhang, 2008).

Holt and Zhang (2008) studied long-term trends of T_i over Millstone Hill (42.6°N, 288.5°E) using the observations of incoherent scatter radar (ISR) from 1978 to 2007. They found a larger negative trend in daytime T_i and T_n (−5 K/year) at 375 km than anticipated from Roble and Dickinson (1989). This trend of T_i matches with that of the St. Santin ISR at the same altitude (Donaldson et al., 2010). Four solar cycles of Millstone Hill ISR data (1968–2006) were analyzed for long-term noontime trends at 100–550 km altitude. A cooling trend was found above 200 km, and it increased with altitude; also, a warming trend was found below 200 km (Zhang et al., 2011). They stated that their results of the long-term trend altitude variation are in agreement with the models predicting the response of the ionosphere to the changes in concentration of GHG.

Zhang and Holt (2013) also used Millstone Hill ISR data to understand the long-term cooling as function of local time, season, solar activity, and geomagnetic activity. They found stronger cooling trends during daytime than nighttime. They also found negligible seasonal variation in the T_i trend, which is in agreement with the seasonal variation of neutral density trends reported by Emmert et al. (2004). Emmert et al. (2004) also studied the dependency of long-trends in density on geomagnetic activity, local time, latitude, and season using the observations of 27 near-Earth space objects over 36 years. They did not find a larger or consistent dependency, whereas Zhang and Holt (2013) found a clear local time dependency. Both of them found solar activity dependency. In Millstone Hill, strong cooling trends were found during solar minimum, whereas less cooling or warming was found during solar maximum. Zhang and Holt (2013) speculated that a fraction of the cooling trend was due to the gradual shifting of Millstone Hill away from the sub-auroral region.

Zhang et al. (2016) analyzed two high-latitude ISR site data sets (Sondrestrom during 1990–2015, and Chatanika/Poker Flat during 1976–2015 with a gap in 1983–2006) for a comprehensive study on long-term trends and a comparison with the Millstone Hill ISR data. They concluded that the upper atmosphere is cooling globally, significantly above 200 km. The cooling trends were much stronger than the Thermosphere-Ionosphere-Mesosphere-Electrodynamics general circulation model (GCM) predicted for the increase in the concentration of GHGs (Qian et al., 2011). Above 275 km, cooling trends have a geomagnetic latitudinal dependency since ISRs estimated T_i trends increase with increasing magnetic latitude. Cooling trends from ion temperature residuals are found in all the altitudes of the ionosphere/upper atmosphere except below ∼175 km.

At lower altitudes of the ionospheric F-region (∼125–175 km), the warming trends are mostly observed at mid-latitude and high-latitudes but at different altitudes. During the daytime, warming trends are occurring below 175 km in Millstone Hill, Sondrestorm, Chatanika/Poker Flat, and Saint Santin (Donaldson et al., 2010; Zhang et al., 2016, 2011). Warming trends were also observed during nighttime at lower altitudes of the ionospheric F-region. During the nighttime, Millstone Hill has a warming trend below 350 km (Zhang & Holt, 2013) and Sondrestorm below 250 km, while at Chatanika/Poker Flat, no data were analyzed below 220 km, and no warming was observed above 220 km (Zhang et al., 2016). These warming trends at fixed altitudes are not due to the true warming of the ionosphere; it is due to the downward shift in pressure level because of the subsidence of warmer air with a substantial altitude gradient in temperature, as is the case for the lower F-region (Akmaev & Fomichev, 1998; Donaldson et al., 2010; Zhang & Holt, 2013; Zhang et al., 2016, 2011). These warming trends occur at the lowest altitudes during the daytime but higher altitudes during nighttime. These occurrences are the same in all the latitude stations except Tromso (Ogawa et al., 2014; Zhang et al., 2016).

Ogawa et al. (2014) used the ISR observations of EISCAT UHF radar in Tromso during 1981–2013 to estimate the ionospheric T_i trends at high latitudes. Moreover, they have found comparable values to the GCM predictions

21699402, 2023, 2, Downloaded from https://agupubs.onlinelibrary.wiley.com/doi/10.1029/2022JA031049, Wiley Online Library on [02/04/2023]. See the Terms and Conditions (https://onlinelibrary.wiley.com/terms-and-conditions) on Wiley Online Library for rules of use; OA articles are governed by the applicable Creative Commons License

of Qian et al. (2011). Their T_i trends are −0.5 to −1.5 K/year at 200–380 km altitude, and −0.5 to 1 K/year at 400–470 km altitude. They stated that their height profiles of observed trends are relatively close to the GCM predictions. In fact, the trends observed by Ogawa et al. (2014) were still somewhat larger than the prediction and are less than those estimated from Millstone Hill and Saint Santin IS radar data.

Cooling trends increase with altitude over Tromso from 230 to 330 km. Above 330 km, cooling trends are decreasing as a function of altitude, and the trends turn into warming at just 410 km. The warming trends increase above 410 km as a function of altitude (Ogawa et al., 2014). The decrease of the cooling trend as a function of altitude was observed at other latitudes too, but in different altitude ranges. It was observed as 325(night)/425(day) - 450 km over Sondrestrom and 325–375 km over Chatanika/Poker Flat. These kinds of reduced cooling trends in altitude profiles more or less occur at the peak altitude of the F-region. It can be noted that only Millstone Hill does not observe any such feature. Rather, Millstone Hill observed increasing cooling trends as a function of altitude, which is found to be in the overall trends of Saint Santin and Chatanika/Poker Flat, too. In contrast, warming trends were observed above the peak altitude of the F-region over Tromso (above 400 km) during the daytime (Ogawa et al., 2014).

There is an attempt to explain the strong T_i trends of ISR data sets by long-term changes in the ion composition of the lower part of the F-region (Perrone & Mikhailov, 2017). The study was made to clear up the two situations, namely, (a) the positive T_i trends below 200 km, and (b) the increasing positive T_i trends with altitude above 400 km. Perrone and Mikhailov (2017) used the June noontime monthly median f_oF_1 to calculate T_{ex} long-term variations from the chain of ionosondes in the European sector, Sodankyla, Juliusruh, and Rome. Perrone and Mikhailov (2017) pointed out that ISR observed a positive T_i trend at 175 km altitude is an overestimation since it should be a negative trend at F_1 region altitudes by the negative trend in mean ion mass. This overestimation is due to the sensitivity of the ISR observations to the T_i/m^+, where m^+ is the mean ion mass. Furthermore, they commented on T_i trends of Ogawa et al. (2014) particularly above 400 km of altitude where the positive trend increases with altitude. Perrone and Mikhailov (2017) pointed out that the decreasing mean ion mass might cause this increasing positive trend above 400 km due to lighter ions of H^+ and He^+, as an overestimation as like F_1 region altitudes.

The discrepancy between model-predicted values and observed cooling trends is not yet fully understood. Lack of understanding in long-term trends could be due to the limited amount of well-calibrated data and its availability (Ogawa et al., 2014). It may need further studies to understand the variability in derived cooling trends as mentioned by Zhang et al. (2016). To bring more light to understanding the long-term trend of ion temperature in the upper atmosphere, we analyzed the T_i data over Arecibo, using Arecibo Observatory incoherent scatter radar (AO-ISR) data sets from 1985 to 2019. We also compared the long-term trends we found in T_i from AO-ISR with the T_i trends from the Whole Atmosphere Community Climate Model eXtension (WACCM-X model). The datasets of WACCM-X were obtained from WACCM-X version 2.0 with the model top at about 400–700 km altitude. This WACCM-X model simulation includes the effects of GHGs and the Earth's magnetic field changes. It also has realistic solar and geomagnetic activity variations. For details on WACCM-X and a description of the simulation setup, the readers are referred to Cnossen (2020a, 2020b, 2022a, 2022b) and Liu et al. (2018). To understand the geomagnetic latitude dependency of T_i trends, we have compared the estimated T_i trends of AO-ISR with those of other ISRs.

2. Data Analysis

We have analyzed the ion temperature (T_i) from ion-line data sets, which were obtained from the AO-ISR (18°20'N, 66°45'W). The AO-ISR ion-line data sets were processed in different ways. We use the data which were processed by the world day standard algorithm. These data sets are available from January 1985 throughout three solar cycles. We use the ISR data from 1985 to 2019 at all zenith angles; the AO-ISR could steer the beam up to 20° of off-zenith, and these data cover all the hours and months as shown in Figure 1, especially in panel (c). ISR data has been missing for 2 years (1996 and 2007), as shown in panel (a). Data gaps are represented by white/blank space in the figure of the year versus month. The hourly median values generate this data distribution. Since AO-ISR observations had different time and altitude resolutions, altitude resolution is fixed to be ∼36 km to bin the T_i data into 16 altitude bins from ∼122 to ∼695 km, centered at 140, 176, 212, 247, 283, 319, 355, 391, 427, 462, 498, 534, 570, 606, 642, and 677 km.

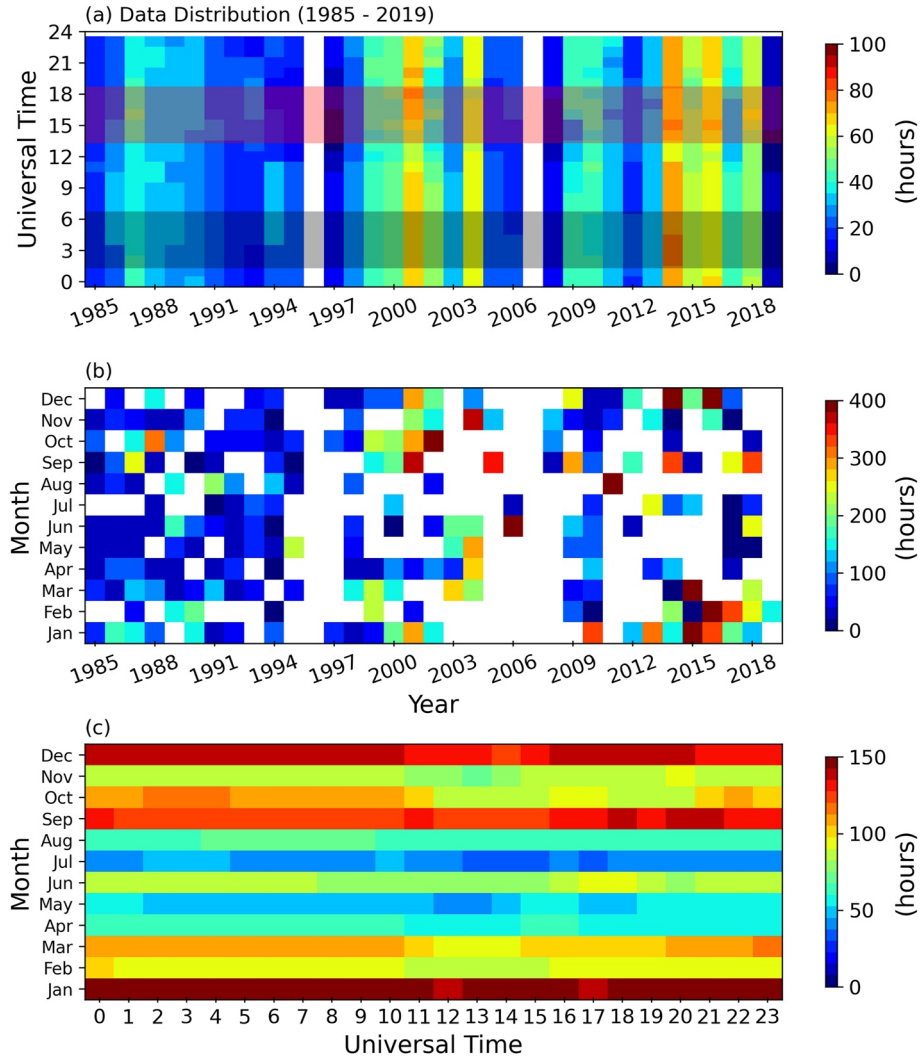

Figure 1. Temporal distribution of ion temperatures from 1985 to 2019 over Arecibo; (a) year versus Universal Time, (b) year versus month, and (c) Universal Time versus month. The scale represents the number of hours of data available for each bin. Horizontal bars in panel (a) represent the local-noon (red) and local-night (black) times.

Climatological models could be less reliable when disturbed geomagnetic conditions or extremely high solar activity exist. To remove such effects, we rejected the T_i values corresponding to the solar flux at 10.7 cm having $F_{10.7} > 300$ sfu and geomagnetic activity having $ap > 80$ nT. Monthly median values of T_i are estimated for the T_i trend calculations to eliminate the issues in observations such as short-term correlations over days/hours, over-sampling, and outliers (Holt & Zhang, 2008; Zhang et al., 2016). In the estimation of T_i trends, these binned T_i data are analyzed by following the methods of Holt and Zhang (2008), and Zhang et al. (2016). In the estimation of monthly median values, the minimum number of data points is set to be more than six points in each altitude bin, as described by Holt and Zhang (2008), and Zhang et al. (2016). For further details, the readers are referred to their papers. These T_i data are binned by altitude and month bins for constructing a T_i model. T_is corresponding to local mid-noon (16 UT) and mid-night (4 UT) are taken within ±3 hr of these times for comparison between day and night as of Zhang et al. (2016).

Figures 2 and 3 show the monthly median of T_i (black dot) for day and night, respectively, at various altitudes, along with the corresponding $F_{10.7}$ and A_p index. The T_i values are within ±3 hr of local noon and local midnight. Day and Night values have a similar dependence on $F_{10.7}$ and A_p index. Red symbols indicate the yearly medians. The variation of T_i shows a strong dependence on $F_{10.7}$. This means that solar activity influences on T_i need to be removed to reveal the trend caused by unknown drivers. The influences of magnetic activity (A_p index) on T_i

21699402, 2023, 2, Downloaded from https://agupubs.onlinelibrary.wiley.com/doi/10.1029/2022JA031049, Wiley Online Library on [02/04/2023]. See the Terms and Conditions (https://onlinelibrary.wiley.com/terms-and-conditions) on Wiley Online Library for rules of use; OA articles are governed by the applicable Creative Commons License

21699402, 2023, 2, Downloaded from https://agupubs.onlinelibrary.wiley.com/doi/10.1029/2022JA031049, Wiley Online Library on [02/04/2023]. See the Terms and Conditions (https://onlinelibrary.wiley.com/terms-and-conditions) on Wiley Online Library for rules of use; OA articles are governed by the applicable Creative Commons License

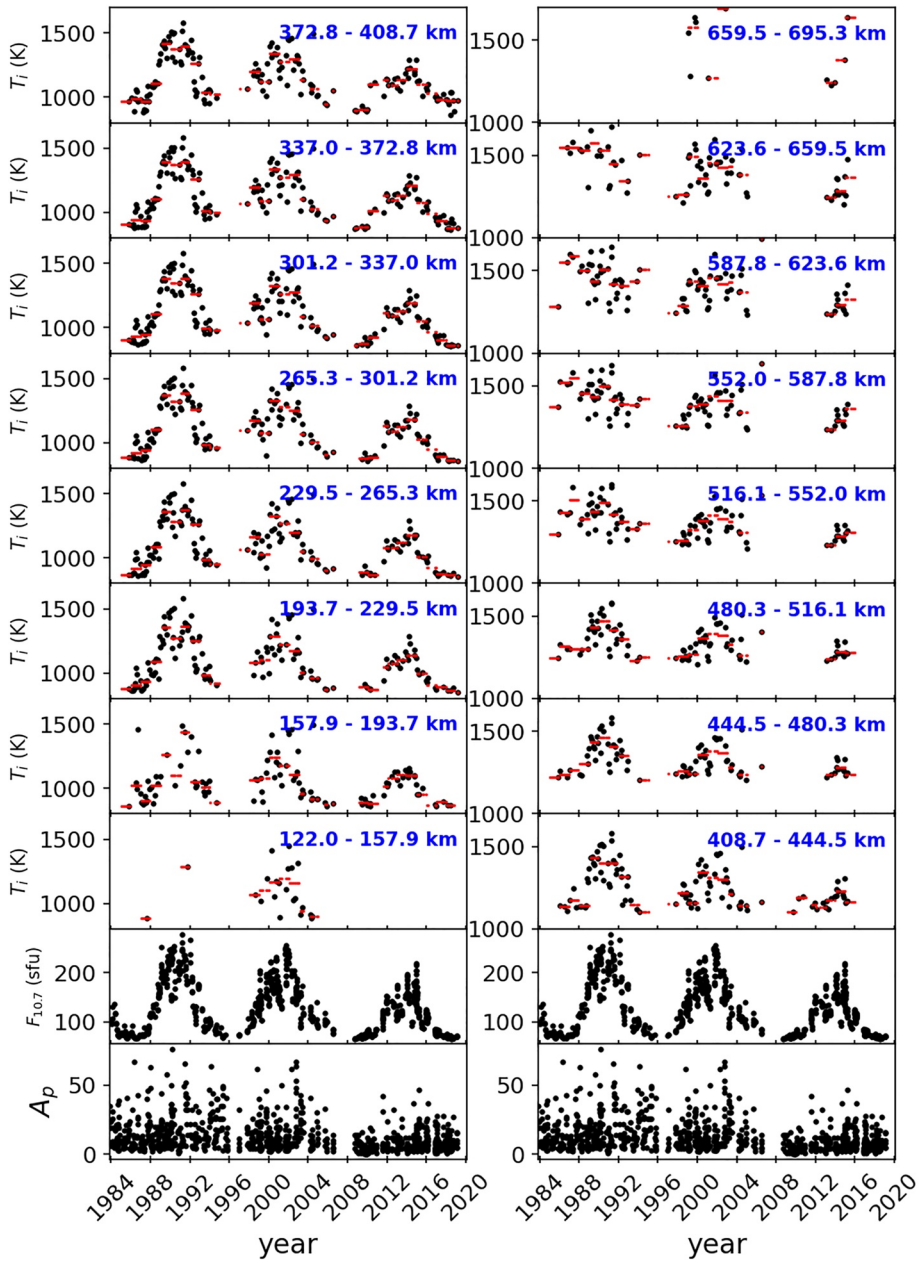

Figure 2. Monthly medians of ion temperature within ±3 hr of local noon (black dot) at various altitudes. The red dashes represent the yearly medians. The two bottom panels of each column are solar flux ($F_{10.7}$) and geomagnetic activity (A_p), corresponding to the study period.

values of AO-ISR are not strong as $F_{10.7}$. But A_p index is a contributor to the T_i values (Holt & Zhang, 2008; Zhang & Holt, 2013; Zhang et al., 2016, 2011). Hence, we will discuss this part in detail in Section 2.2. Continuous observations of T_i are not available all the day and night. Thus, there are data gaps, especially above ∼660 km during the day and below ∼158 km during the day and night. Those altitude ranges are included instead of removed to maintain consistent altitude ranges in day and night.

2.1. Estimation of T_i Residuals

For a given altitude bin, T_i variations are modeled for each time (month) bin based on the least squares fitting using the monthly median of the ISR observed T_i, the monthly median of solar flux at 10.7 cm, A_p index, annual-

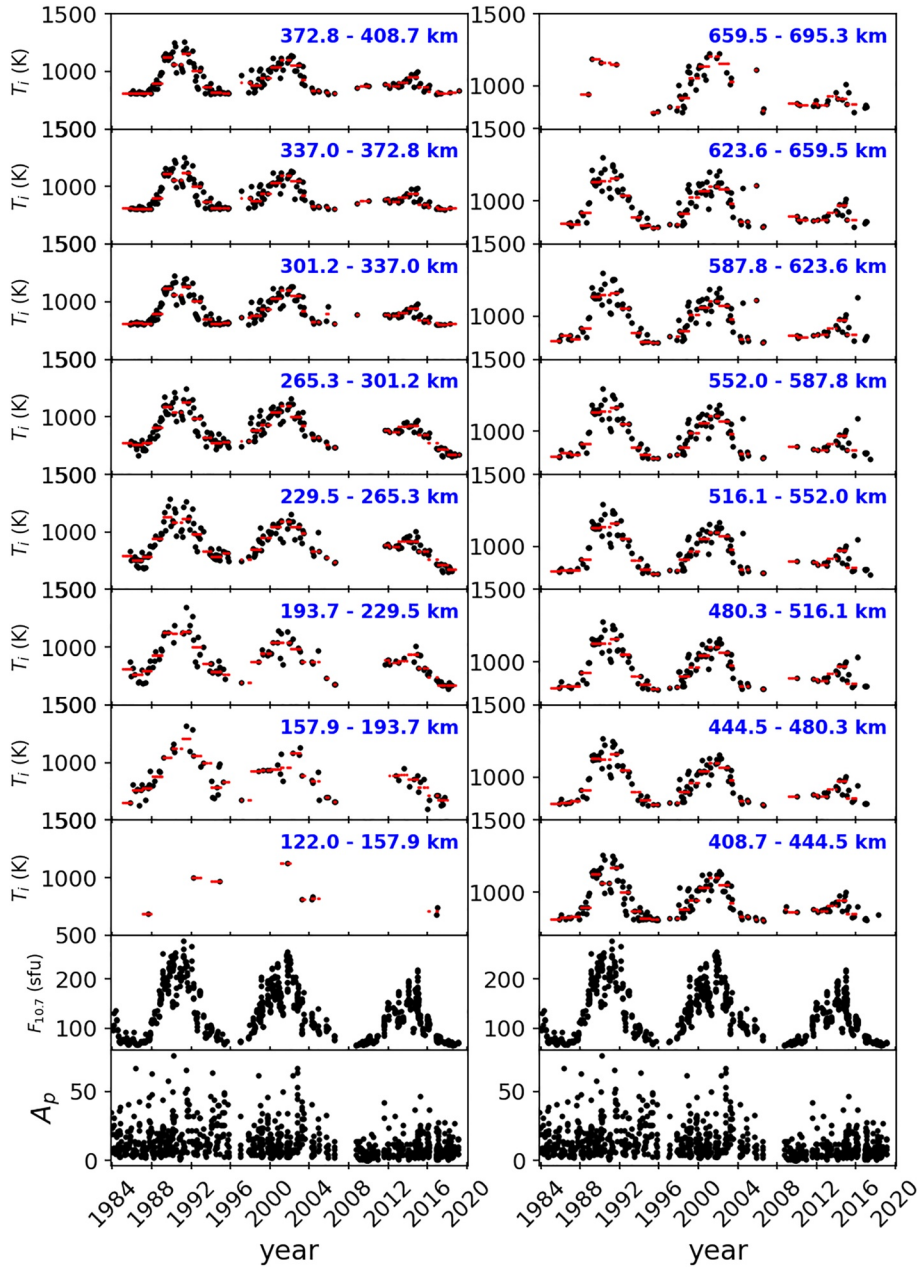

Figure 3. Same as Figure 2 but for local mid-night.

and semi-annual oscillations (Holt & Zhang, 2008; Zhang & Holt, 2013; Zhang et al., 2016, 2011). The variation of T_i is modeled based on the equation given by Zhang et al. (2016), as shown in Equation 1, while Equation 2 describes the fitting residuals, discussed below.

$$T_i = T_b + t(y - \bar{y}) + \sum_{n=1}^{2}\left[a_n \sin(2\pi nd/365) + b_n \cos(2\pi nd/365)\right] + \left(f_1\left(F_{10.7} - \overline{F_{10.7}}\right) + f_2\left(F_{10.7} - \overline{F_{10.7}}\right)^2\right) + a\left(Ap - \overline{Ap}\right) + R \quad (1)$$

$$R_t = T_i - \left(T_b + \sum_{n=1}^{2}\left[a_n \sin(2\pi nd/365) + b_n \cos(2\pi nd/365)\right] + \left(f_1\left(F_{10.7} - \overline{F_{10.7}}\right) + f_2\left(F_{10.7} - \overline{F_{10.7}}\right)^2\right) + a\left(Ap - \overline{Ap}\right)\right) \quad (2)$$

21699402, 2023, 2, Downloaded from https://agupubs.onlinelibrary.wiley.com/doi/10.1029/2022JA031049, Wiley Online Library on [02/04/2023]. See the Terms and Conditions (https://onlinelibrary.wiley.com/terms-and-conditions) on Wiley Online Library for rules of use; OA articles are governed by the applicable Creative Commons License

21699402, 2023, 2, Downloaded from https://agupubs.onlinelibrary.wiley.com/doi/10.1029/2022JA031049, Wiley Online Library on [02/04/2023]. See the Terms and Conditions (https://onlinelibrary.wiley.com/terms-and-conditions) on Wiley Online Library for rules of use; OA articles are governed by the applicable Creative Commons License

where, T_b is the background constant term; y is the floating-point year; $\overline{y}$ is the mean floating year, t is the long-term trend, d is the day number of the year, $F_{10.7}$ is the monthly solar flux in sfu, $\overline{F_{10.7}}$ is the mean of the solar flux over the entire time series, A_p is the A_p index in nT, $\overline{A_p}$ is the mean of the A_p index over the entire time series, and R is the fitting residual. The coefficients T_b, t, a_n, b_n, f_1, f_2 and a are estimated for each altitude bin by the least squares fitting method.

For a given component (long-term trend /$F_{10.7}$ /A_p index), the T_i residuals are obtained by removing the contribution of the other two components (estimated) from the ISR observed T_i in addition to the seasonality. The detailed procedures to obtain the T_i residuals are given in Holt and Zhang (2008), Zhang and Holt (2013), and Zhang et al. (2016, 2011). For example, the T_i residuals for the component of the long-term trend (R_t) are given in Equation 2. It shows that the trend term lies within the residuals in order to obtain the trend by the curve fit. In order to make the comparison of T_i trends among the ISR sites, a similar method has been used in this study for 95% confidence intervals estimations also, as in Holt and Zhang (2008), Zhang and Holt (2013), and Zhang et al. (2016, 2011). In the estimation of 95% confidence intervals, 10,000 bootstrap samples are used.

2.2. The Dependence of T_i Trends on the Quadratic Term of $F_{10.7}$ and A_p

In the modeling of T_i variations, as mentioned above, we used the formula of Zhang et al. (2016) to compare our T_i trends over Arecibo with their T_i trends of other ISR sites. From Figures 2 and 3, we find a strong dependence of T_i on the solar activity term of $F_{10.7}$. Hence, $F_{10.7}$ is an unavoidable contributor to the T_i variations but such strong dependence of T_i on the geomagnetic activity term (A_p) is not very clear specifically at Arecibo latitudes (but could be significant at higher latitudes). In Equation 1, solar activity ($F_{10.7}$) contributes to two terms in the modeling of T_i variations; one is the linear term $\left(f_1\left(F_{10.7}-\overline{F_{10.7}}\right)\right)$ and the another one is the quadratic term $\left(f_2\left(F_{10.7}-\overline{F_{10.7}}\right)^2\right)$. Further, the geomagnetic activity (A_p) also contributes to the modeling of T_i variations. However, such a strong dependence of T_i on A_p is not very clear, and the role of the quadratic term of the $F_{10.7}$ flux variations is not easily understood. Therefore, we demonstrate the dependence of T_i trends on A_p and the quadratic term of $F_{10.7}$. In order to do that, we re-write Equation 2 of the T_i residuals for the component of the long-term trend to check the influence of additional/removal of A_p and quadratic term of $F_{10.7}$ on estimated T_i trends, as follows:

$$R_{t_{-\left(f_2\tilde{F}^2_{10.7}+a\tilde{A}_p\right)}} = T_i - \left(T_b + \sum_{n=1}^{2}\left[a_n\sin(2\pi nd/365) + b_n\cos(2\pi nd/365)\right] + f_1\left(F_{10.7}-\overline{F_{10.7}}\right)\right) \quad (3)$$

$$R_{t_{-\left(f_2\tilde{F}^2_{10.7}\right)}} = T_i - \left(T_b + \sum_{n=1}^{2}\left[a_n\sin(2\pi nd/365) + b_n\cos(2\pi nd/365)\right] + f_1\left(F_{10.7}-\overline{F_{10.7}}\right) + a\left(Ap-\overline{Ap}\right)\right) \quad (4)$$

$$R_{t_{-\left(a\tilde{A}_p\right)}} = T_i - \left(T_b + \sum_{n=1}^{2}\left[a_n\sin(2\pi nd/365) + b_n\cos(2\pi nd/365)\right] + f_1\left(F_{10.7}-\overline{F_{10.7}}\right) + f_2\left(F_{10.7}-\overline{F_{10.7}}\right)^2\right) \quad (5)$$

where, $\tilde{F}^2_{10.7} = \left(F_{10.7}-\overline{F_{10.7}}\right)^2$ and $\tilde{A}_p = Ap - \overline{Ap}$.

The T_i residuals for the component of the long-term trends are shown in Equations 3–5. Equation 3 calculates the residuals by modeling the T_i without A_p and the quadratic term of $F_{10.7}$. It means the resulted T_i residuals contain the contributions of the long-term trend, A_p and the quadratic term of $F_{10.7}$ in it. Equation 4 calculates the residuals by modeling the T_i without the quadratic term of $F_{10.7}$. It means the resulted T_i residuals contain the contributions of long-term trend and the quadratic term of $F_{10.7}$ in it. Equation 5 calculates the residuals by modeling the T_i without A_p. It means the resulted T_i residuals contain the contributions of long-term trend and A_p in it.

In addition to the T_i residuals for the component of the long-term trend, we have also calculated the T_i residuals for the component of $F_{10.7}$(the contribution of $F_{10.7}$ to T_i is not removed, but the contribution of the long-term

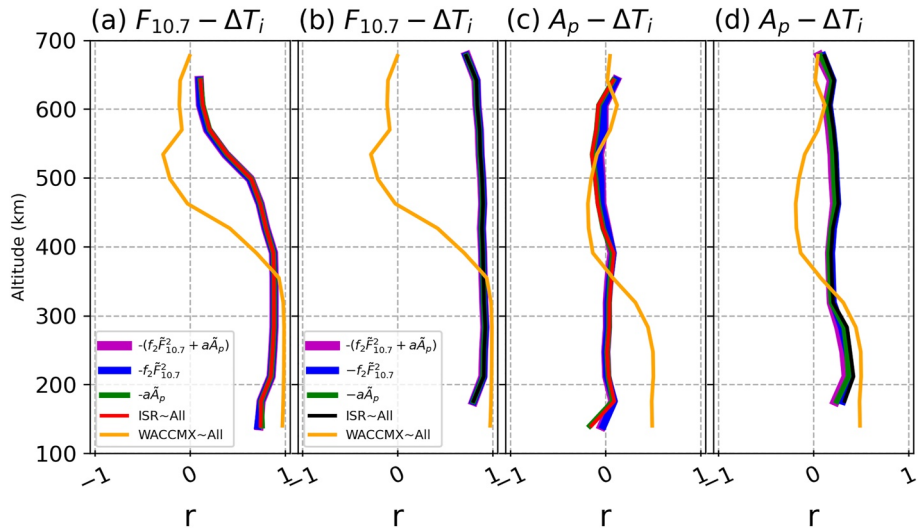

Figure 4. The correlation coefficients as a function of altitude. (a) Correlation between $F_{10.7}$ and T_i residuals for day, (b) correlation between $F_{10.7}$ and T_i residuals for night, (c) correlation between A_p and T_i residuals for day, and (d) correlation between A_p and T_i residuals for night.

trend and A_p are removed from ISR observed T_i) and for the component of A_p (the contribution of A_p to T_i is not removed but the contribution of long-term trend and $F_{10.7}$ are removed from ISR observed T_i) to estimate the correlation coefficients. In the comparison of correlation coefficients among different cases, T_i of WACCM-X is also included for the sake of comparison between the model and observations. For the comparison of the model (WACCMX~All) and observation (ISR~All), the T_i residuals are also estimated without removing any terms (quadratic term of $F_{10.7}$ / A_p) from the T_i model. From WACCM-X, the monthly mean T_i values are obtained for the locations of Arecibo in the time period of January 1985 to February 2019 at the same altitude levels as AO-ISR. These monthly values do not distinguish between day and night; therefore, it represents the whole day and night together.

Figure 4 shows the correlation coefficients between $F_{10.7}$ and T_i residuals for (a) day and (b) night, and the correlation coefficients between A_p and T_i residuals for (c) day and (d) night. Figures 4a and 4b represent the correlation coefficients calculated between $F_{10.7}$ and T_i residuals by using the T_i models without (Equation 3) A_p and quadratic term of $F_{10.7}$ (pink-line), (Equation 4) quadratic term of $F_{10.7}$ (blue-line), and (Equation 5) A_p (green-line). The red-line (ISR~All - day), black-line (ISR~All - night), and orange-line (WACCMX~All - whole day) represent the correlation coefficients calculated without removing any terms from the T_i model. Figures 4c and 4d represent the correlation coefficient between A_p and T_i residuals without (Equation 3) A_p and quadratic term of $F_{10.7}$ (pink-line), (Equation 4) quadratic term of $F_{10.7}$ (blue-line), and (Equation 5) A_p (green-line) in the estimation of T_i variations. The red-line (daytime), black-line (nighttime) (ISR~All), and orange-line (WACCMX~All - whole day) represent the correlation coefficients which are calculated without removing any term from the T_i model.

In Figure 4a, the correlation coefficients (r) during daytime vary from 0.8 to 0.9 in the altitudes of ~220–400 km. Above the ~400 km, it decreases as a function of altitude. In Figure 4b, the nighttime correlation coefficients vary from 0.8 to 0.93 within altitudes of ~220–650 km. During day and night, there is no significant difference among different cases resulting from adding/removing A_p and the quadratic term of $F_{10.7}$. Unlike the daytime, the values of r during the night are gradually decreasing as a function of altitude for small changes. The correlation coefficients of WACCM-X (WACCMX~All) between $F_{10.7}$ and the T_i residuals are found to be as high as 0.99. The values of r decrease as a function of altitude above ~300 km and are negative above ~450 km altitude.

In Figure 4c, the correlation coefficients (r) during daytime vary within the range of −0.15 to 0.1 in most altitudes. In particular, a positive correlation is observed below ~400 km altitude, and a negative correlation is observed above ~400 km altitude. The correlation is very poor in the case of modeled T_i variations without A_p and the quadratic term of $F_{10.7}$ (pink-line). Almost the same poor correlation is found in the case of modeled T_i variations without the quadratic term of $F_{10.7}$ (blue-line) but with A_p. A slight improvement in correlation is seen in the case of modeled T_i variations with a quadratic term of $F_{10.7}$ but without A_p. There is more improvement

21699402, 2023, 2, Downloaded from https://agupubs.onlinelibrary.wiley.com/doi/10.1029/2022JA031049, Wiley Online Library on [02/04/2023]. See the Terms and Conditions (https://onlinelibrary.wiley.com/terms-and-conditions) on Wiley Online Library for rules of use; OA articles are governed by the applicable Creative Commons License

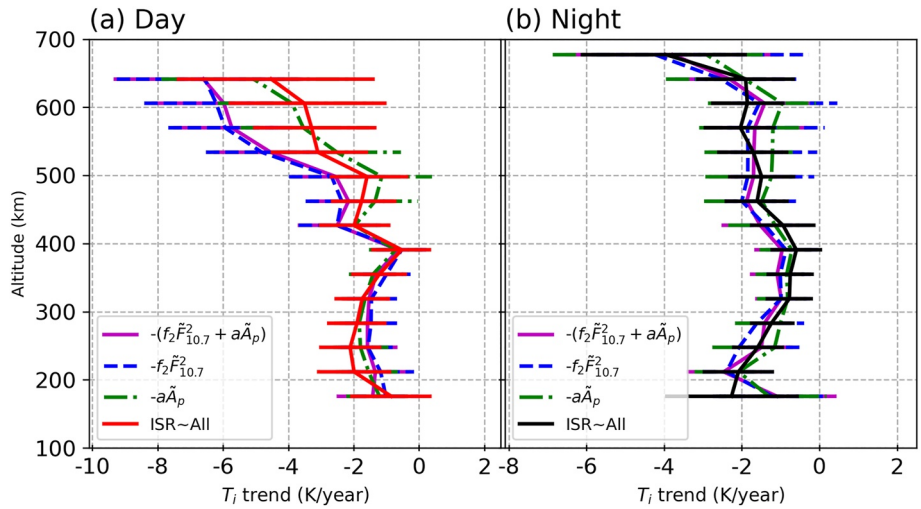

Figure 5. The T_i trends as a function of altitude. Pink represents the trend from the T_i model without A_p and quadratic term of $F_{10.7}$; blue represents the trend from the T_i model without the quadratic term of $F_{10.7}$; green represents the trend from the T_i model without A_p; red (day) and black (night) represents the trend from T_i model with all terms.

in correlation coefficients in the case of modeled T_i variations without removing any terms from the model (ISR~All in red-line). This behavior is observed at nighttime (ISR~All in black-line), too, even though the magnitudes of r are not comparable to the same of daytime. However, the nighttime r values are positive in all the altitudes and higher (0.43) than the daytime. The correlation coefficients of WACCM-X (WACCMX~All) between A_p and T_i residuals are found to be as high as 0.51, they have a feature similar to the daytime values of ISR~All in the sense of changing the r values from positive to negative. The values of r decrease as a function of altitude above ~300 km and have negative values above ~450 km altitude. Overall, there is no significant differences among the correlation coefficients among different cases. And no significant correlation is found between ion temperature and geomagnetic activity using AO-ISR over Arecibo. Based on these demonstrated results, one can neglect the geomagnetic activity removal in the estimation of T_i trends over Arecibo. To understand further the influence of geomagnetic activity and the quadratic term of $F_{10.7}$ on the estimated T_i trends, it may be interesting to see the comparison of T_i trends among those cases before removing the geomagnetic activity term.

The comparison of T_i trends among those different cases is shown in Figure 5. Notably, there is no significant difference in 95% confidence intervals among those different cases. The confidence intervals vary in their trend values. These variations in the trend values are mostly from 0.8 to 1 K/year below ~400 km altitude, and those are more than 1 K/year above ~400 km altitude during the daytime period. It is similar but has a little smaller range in the nighttime than in the daytime. Generally, the confidence intervals increase with altitude. These values of the confidence intervals for the altitudes below 550 km are closely matching with those of Millstone Hill ISR observations during 1978–2007 (~1.1 K/year about the T_i trend), 1968–2006 (~0.75 K/year about the T_i trend) and 1980–2006 (~1.5 K/year about the T_i trend; Holt & Zhang, 2008; Zhang et al., 2011).

The notable differences in T_i trends are found among those different cases during day and night. In Figure 5a, relatively weaker cooling trends are found below ~400 km altitude for the case of modeled T_i variations without the quadratic term of $F_{10.7}$ (blue-line). Above the altitude of ~400 km, cooling trends are very stronger in this case and also get stronger as a function of the altitude. Removal of the quadratic term of $F_{10.7}$ leads to weak cooling trends in the altitudes below ~400 km and strong cooling trends in the altitudes above ~400 km. Removal of both A_p and quadratic term of $F_{10.7}$ from the T_i model causes more strong cooling below ~400 km and relatively weak cooling above ~400 km altitude. Removal of A_p from the T_i model leads to a relatively strong cooling below ~400 km altitude, whereas it results in weaker cooling above ~400 km altitude. Removal of A_p affects the trend profile, especially near ~230 km altitude and above ~400 km altitude during daytime and nighttime. During the nighttime, weaker cooling trends are found by the removal of A_p, and stronger cooling trends are found by the removal of the quadratic term of $F_{10.7}$. In comparison, T_i is more sensitive to A_p during nighttime due to the absence of solar EUV (Extreme Ultra-Violet) than during the daytime. In contrast, both day and night times of T_is are highly sensitive to the quadratic term of $F_{10.7}$.

21699402, 2023, 2, Downloaded from https://agupubs.onlinelibrary.wiley.com/doi/10.1029/2022JA031049, Wiley Online Library on [02/04/2023]. See the Terms and Conditions (https://onlinelibrary.wiley.com/terms-and-conditions) on Wiley Online Library for rules of use; OA articles are governed by the applicable Creative Commons License

21699402, 2023, 2, Downloaded from https://agupubs.onlinelibrary.wiley.com/doi/10.1029/2022JA031049, Wiley Online Library on [02/04/2023]. See the Terms and Conditions (https://onlinelibrary.wiley.com/terms-and-conditions) on Wiley Online Library for rules of use; OA articles are governed by the applicable Creative Commons License

In all cases, T_i trends are generally found to be cooling in all altitudes. Weakening and strengthening of cooling trends are found to appear in different cases. Even though there is no significant correlation found between ion temperature and geomagnetic activity, there is an influence of geomagnetic activity on the estimated T_i trends. This means that solar and magnetic activity influences on T_i need to be removed to reveal the trend caused by unknown drivers. Hence, we use all the terms of Equation 1 in further analysis of T_i trends to avoid just before mentioned biases and have an identical formula to compare T_i trends with other ISR sites.

3. Results

3.1. T_i Trends From AO-ISR

The T_i residuals are presented in Figures 6 and 7 for daytime and nighttime, respectively. The T_i residuals are calculated by removing the contributions from the annual and semi-annual oscillations, as well as the effects of solar and geomagnetic activity. In Figures 6 and 7, T_i residuals (monthly median-black and yearly median-green) are shown at various altitudes from ∼122 to 700 km along with the number of months (No.), trend line (solid black line), and their slope (m) (corresponding to the 50th percentile), 97.5th percentile (confidence level of 95%), and correlation coefficient (r) between T_i residuals and floating year. The confidence level of 95% is calculated from 10,000 bootstrap samples, and the 97.5th percentile is shown in figure for each altitude. The 97.5th percentile means that 97.5% of the bootstrap samples have trend values at that percentile or less. At the lowest and highest altitudes (centering altitudes of ∼140 and 677 km) during the daytime, the trend values are not significant since the trend values at 50th (represented by m) and 97.5th percentile are largely different. These large deviations between the 50th and 97.5th percentile are associated with too few data points; even the data points in those altitudes do not cover the three solar cycles as in other altitudes. We eliminate these altitudes with few data points and large deviations between the 50th and 97.5th percentile in further analysis to avoid the biased interpretations of trends. The T_i residuals spread around the trend line, meaning those residuals are the origin of ionospheric weather rather than statistical noise. All the altitudes have clear, significant cooling T_i trends from ∼158 to ∼660 km (from ∼158 to ∼695 km) during daytime (nighttime) except a few altitude bins of ∼157.9–193.7 km (during daytime) and ∼372.8–408.7 km (during daytime and nighttime) have negligible cooling trends.

In Figure 6, those cooling T_i trends vary from −0.53 to −4.53 K/year during the daytime. Strong cooling of −4.53 K/year occurs at the altitude bin of ∼623.6–659.5 km, where high values of 97.5th percentile are seen. The weakest or even negligible cooling of −0.53 K/year is happening at ∼372.8–408.7 km with the 97.5th percentile of 0.31 K/year. Altitudes above ∼516 km mostly have relatively larger values of 97.5th percentile (−2 K/year) than lower altitudes.

During the nighttime, the first lower altitude bin does not have enough samples (∼122–158 km) to estimate the long-term trends; the available samples are shown in Figure 3. In all the altitudes, significant cooling trends are found (from ∼158 to 695 km) except in one altitude bin of ∼372.8–408.7 km. These cooling T_i trends vary from −0.6 to −3.96 K/year during the nighttime. Strong cooling of −3.96 K/year occurs at the altitude bin of ∼659.5–695.3 km with the 97.5th percentile of −1.92 K/year. The negligible cooling of −0.6 K/year occurs at the altitude bin of ∼372.8–408.7 km with the 97.5th percentile of 0.02 K/year.

The 95% confidence intervals lie within the range of −7.4 to 0.31 K/year during daytime (−6.1 to 0.02 K/year during nighttime). These values mainly represent cooling trends except for the two (one) altitude bins during daytime (nighttime), which have small positive values at ∼157.9–193.7 km (during the day) and ∼372.8–408.7 km (during day and night). Generally, the trend magnitudes and the 95% confidence intervals on the average increase with altitude in the altitudes above ∼400 km and decrease with altitude till ∼400 km altitude during day and night.

Estimated mean (50th percentile) T_i trends are negative in all the altitudes indicating overall cooling trend of the overall ionosphere during day and night. T_i trends are almost equal between day and night in overlapping altitudes of (centered at) 212, 391, 462, and 498 km. Generally, strong T_i cooling trends are mostly found to be in the daytime than nighttime, and those differ by almost ∼1 K/year in altitudes less than ∼500 km.

3.2. The Residual Solar Cycle Influences on T_i Trends

In estimating long-term trends, one of the most significant factors affecting the trend estimates is the removal of the solar cycle (Clilverd et al., 2003; Cnossen, 2020a). Cnossen (2020a) presented the global mean neutral

21699402, 2023, 2, Downloaded from https://agupubs.onlinelibrary.wiley.com/doi/10.1029/2022JA031049, Wiley Online Library on [02/04/2023]. See the Terms and Conditions (https://onlinelibrary.wiley.com/terms-and-conditions) on Wiley Online Library for rules of use; OA articles are governed by the applicable Creative Commons License

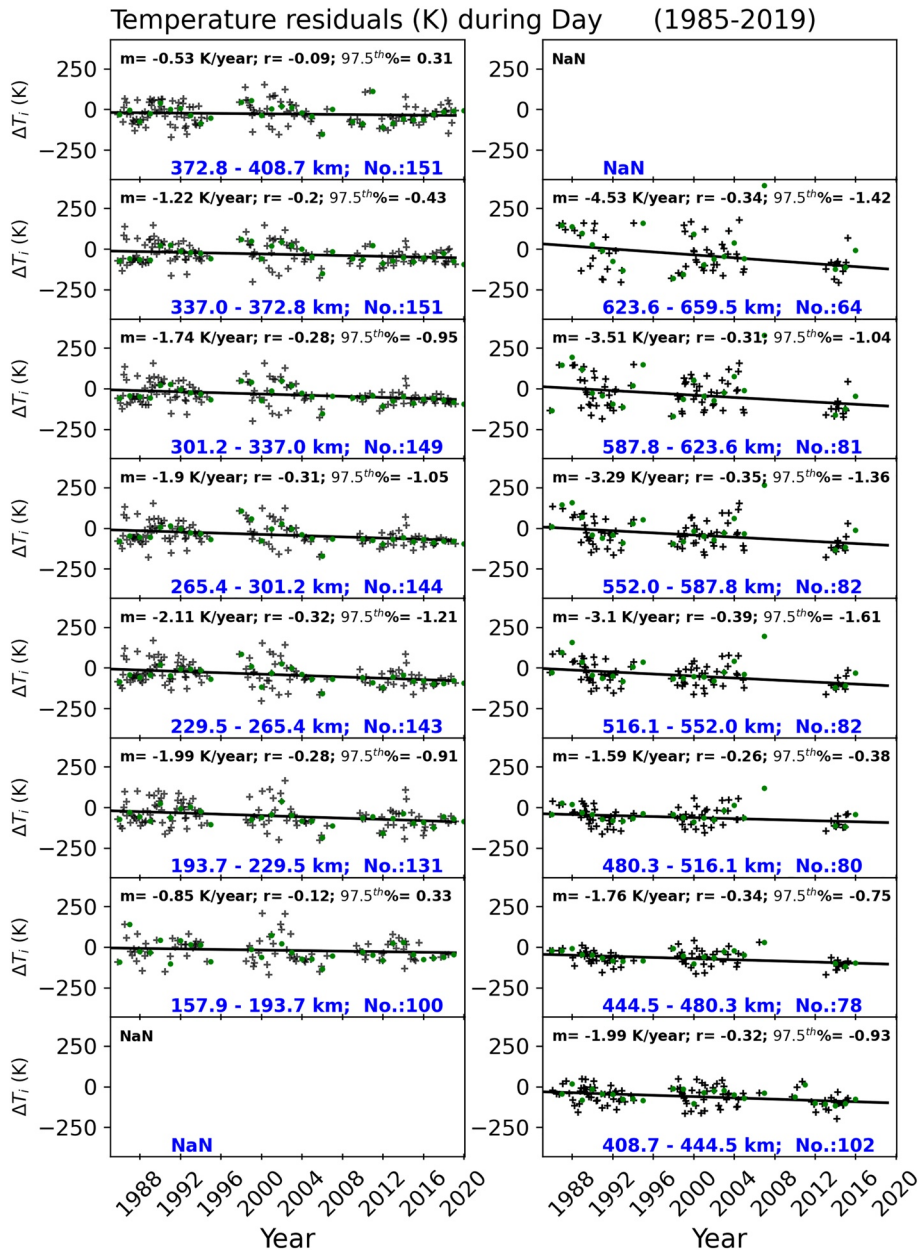

Figure 6. Daytime T_i Residuals as a function of year and altitude along with trend line (solid black line) and its statistics (slope (m), 97.5th percentile, and correlation coefficient (r) between T_i and floating year). Monthly medians are in black crosses, and yearly medians are in green crosses.

temperature (T_n) trends at 400 km from WACCM-X. Furthermore, she demonstrated the influence of solar cycle variations on the estimated T_n trends. In this study, we use T_i of AO-ISR over Arecibo instead of the global mean of T_n. Therefore, we check the influence of solar cycle variations on the estimated T_i trends from WACCM-X model over Arecibo in addition to the AO-ISR observations since there is no other study to compare the observations with the model based on T_i trends. As Cnossen (2020a) did, we also check for any issue with the appropriate removal of solar cycle influences by following their methods. For this purpose, we calculate the long-term trends for a minimum of two solar cycles, from 1985 to the end years (2008–2019).

Figure 8 shows the time evolution of the T_i trends for (a) day and (b) night at various altitudes from 158 to 516 km. During the day, cooling trends occur at all times, and the cooling trends get stronger over time at all altitudes except ∼157.9–193.7 km and ∼372.8–408.7 km. Nighttime also has such features in addition to the warming

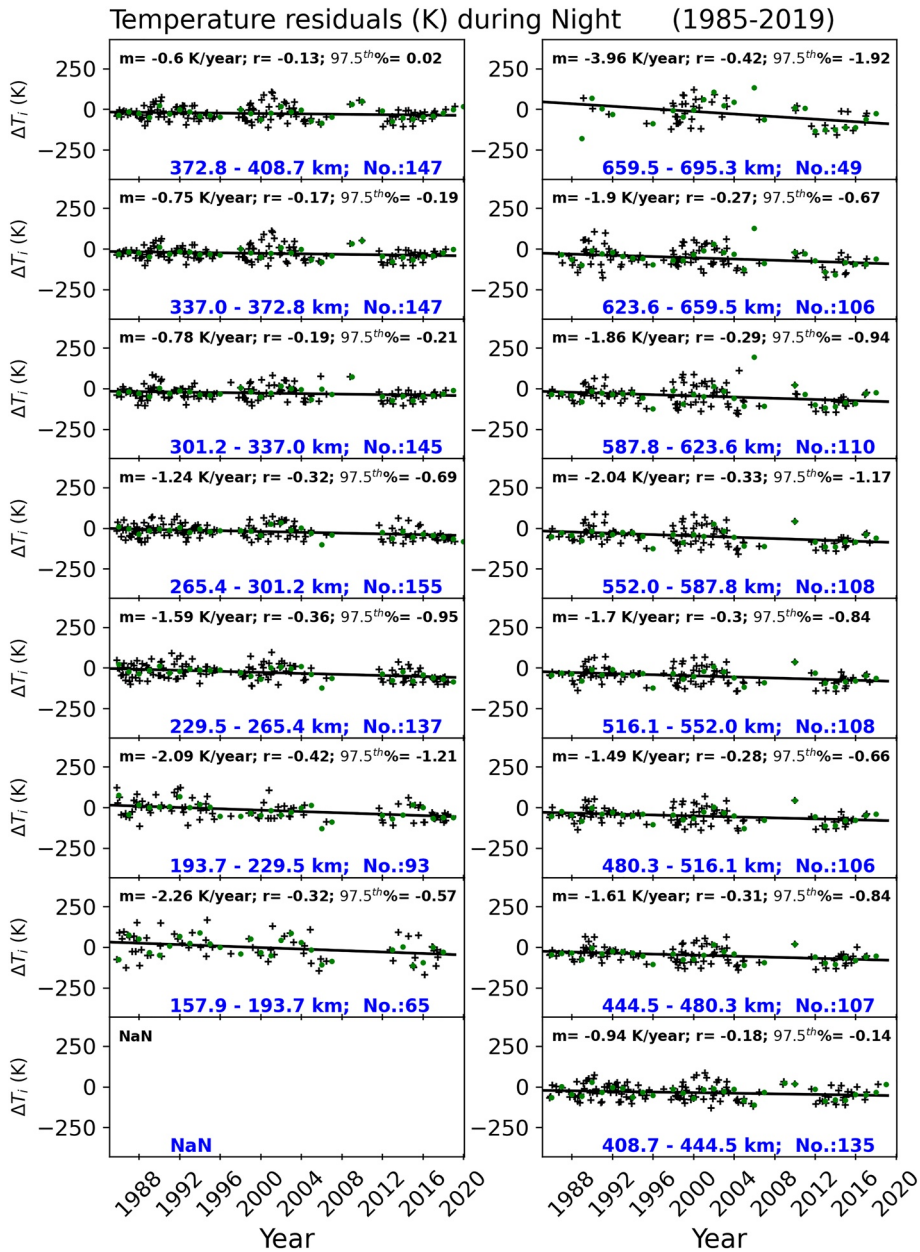

Figure 7. Same as Figure 6 but for the nighttime.

trends for the four end years from 2008 to 2011 at the altitudes of ~265.4–337 km and the weakening of cooling trends over time. Mostly, large variations in the magnitude of the trends and their 95% confidence intervals occur from 2008 to 2013. Since 2013 (2014), the variations have been mostly small during the day and night. These variations are getting smaller and smaller when the trends are approaching the end year of 2018/2019.

The time evolution of the T_i trends from AO-ISR shows a flat line structure after ~the end year of 2014. It is insufficient to state that the formulation used in this study removed the influence of solar cycle variations since the number of end years is not large enough as in Cnossen (2020a) results. For this reason, we use the time evolution of the T_i trends from WACCM-X over Arecibo and Millstone Hill instead of the global mean neutral temperature. WACCM-X model trends over Arecibo are for the same period as the AO-ISR. Furthermore, WACCM-X model trends over Millstone are for the same period of Millstone Hill's ISR (1968–2015) mentioned in Zhang et al. (2016). Millstone Hill's time duration covers more than half of the total number of end years of Cnossen (2020a). Figure 9 shows the time evolution of the T_i trends from WACCM-X over (a) Arecibo and (b)

21699402, 2023, 2, Downloaded from https://agupubs.onlinelibrary.wiley.com/doi/10.1029/2022JA031049, Wiley Online Library on [02/04/2023]. See the Terms and Conditions (https://onlinelibrary.wiley.com/terms-and-conditions) on Wiley Online Library for rules of use; OA articles are governed by the applicable Creative Commons License

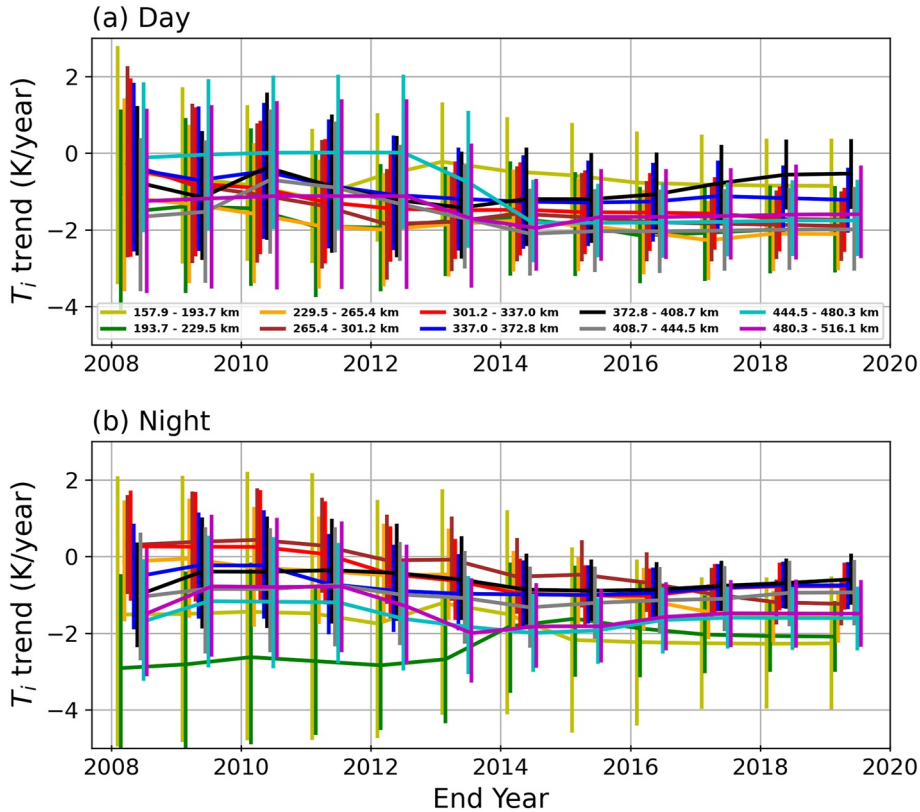

Figure 8. The time evolution of the T_i trends at various altitudes during (a) Day and (b) Night.

Millstone Hill at various altitudes from 158 to 409 km. Above the altitude of 409 km, the confidence intervals are large, hiding the trends in the lower altitudes than 409 km. Thus, the time evolution of the T_i trends for altitudes more than 409 km are not shown here. The flat horizontal line structures are primarily observed in WACCM-X over Arecibo and Millstone Hill, even though the trends in high altitudes have variations of ∼1 K/year as a maximum. Compared with the time evolution of global mean neutral temperature from WACCM-X, T_i trends are horizontally flat, varying ∼1 K/year during 1998–2015, whereas global mean neutral temperature varies ∼3 K/year during 1998–2015. Hence, no significant or noticeable ringing effect is found in T_i trends by the inappropriate removal of solar cycle variations.

At 400 km, global mean neutral temperature trends from WACCM-X fall from −4 K/year at the end year of 2008 to −5.8 K/year at the end year of 2014 (Cnossen, 2020a). That drop of −1.8 K/year is not seen in AO-ISR trends at the corresponding altitude bin of ∼372.8–408.7 km, and also, such a monotonic drop in trends with a decline of −1.8 K/year is not seen during 2008–2014 within the altitudes of 400 km or less. After the 2008/2009 solar minimum, there is a large potential influence of weak solar activity on the trends (Cnossen, 2020a). Those effects may vanish over time in ISR observations since the variations are getting smaller, and flat-horizontal line features are also seen at most of the altitudes when approaching 2018/2019. Hence, the trends estimated at the end year of 2019 would be a good representative of the long-term trends.

3.3. Comparison of T_i Trends

Long-term trends of the ion temperature from multiple ISR locations show variations in magnetic latitude (Zhang et al., 2016). It is useful to compare the AO-ISR trends with those reported from other ISRs because it is at geomagnetic midlatitudes, while the others are higher in latitude. Figure 10 shows the comparison of long-term trends of ISR measured T_i among various ISR locations along with trends of the WACCM-X model for Arecibo and Millstone Hill (red-daytime AO, gray-nighttime AO, black - WACCM-X model for Arecibo, pink-Millstone, sky blue - WACCM-X model for Millstone Hill, green-St. Santin, yellow-Poker Flat, and blue-Sondrestrom). In

21699402, 2023, 2, Downloaded from https://agupubs.onlinelibrary.wiley.com/doi/10.1029/2022JA031049, Wiley Online Library on [02/04/2023]. See the Terms and Conditions (https://onlinelibrary.wiley.com/terms-and-conditions) on Wiley Online Library for rules of use; OA articles are governed by the applicable Creative Commons License

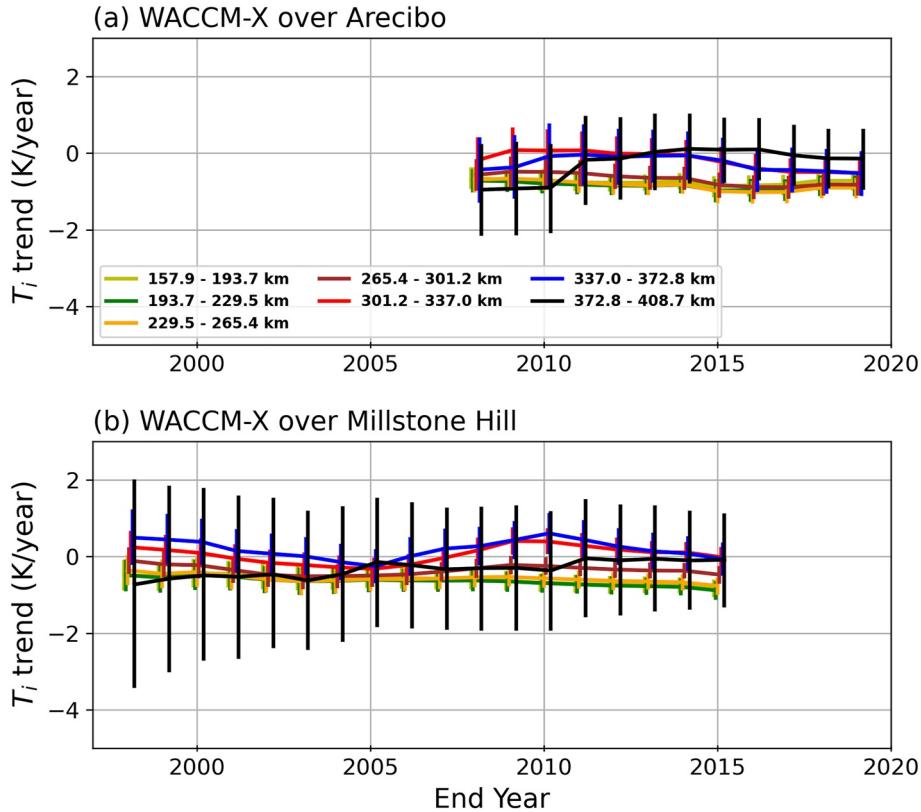

Figure 9. The time evolution of the T_i trends from Whole Atmosphere Community Climate Model eXtension (WACCM-X) model at various altitudes over (a) Arecibo and (b) Millstone Hill.

Figure 10, the observed T_i trends of the listed facilities (daytime) are shown as a function of altitude along with nighttime AO-ISR and WACCM-X model for the entire day and night. The trends from facilities other than Arecibo are from Zhang et al. (2016). As discussed earlier, the error bars from all ISRs represent the 95% confidence intervals corresponding to the 2.5th and 97.5th percentile. As seen in Figure 10, the large confidence intervals are found in AO-ISR than in any other ISRs, but those are comparable to the Millstone Hill ISR observations during different time periods (Holt & Zhang, 2008; Zhang et al., 2011). Even those large confidence intervals exist in the WACCM-X model above ~400 km altitude at the ISR locations of Arecibo and Millstone Hill.

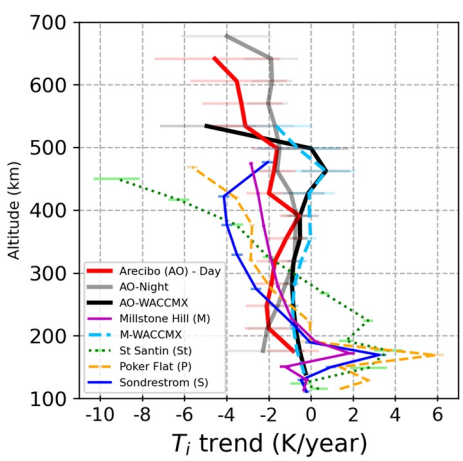

Figure 10. Comparison of T_i trend variations among the Incoherent Scatter Radars (ISRs), namely, Millstone Hill (pink), St. Santin (green), Poker Flat (yellow), Sondrestrom (blue) and Arecibo (red-day and gray-night). The black and sky blue represent the T_i trends from the Whole Atmosphere Community Climate Model eXtension (WACCM-X) model at the ISR locations of Arecibo and Millstone Hill, respectively.

From the ISRs measured T_is, cooling trends are observed above 200 km except at St. Santin, which only shows a cooling trend above 300 km altitude. Almost all cooling trends increase with altitude, but Arecibo has a different feature instead of simply increasing with altitude. Warming T_i trends are observed within the altitude range of 100–200 km in the data from all facilities other than Arecibo. Over Arecibo, the cooling trend is seen in that particular altitude range but is small during the day and strong during the night. Zhang et al. (2016) observed increases in the cooling trend with increasing magnetic latitudes above 275 km except for St. Santin. It could be a geographic latitude dependency if St. Santin is excluded. Since St. Santin data was collected from 1966 to 1987 when global warming signals at the surface had just started and data coverage is too short for long-term trends (Zhang et al., 2016); hence, St. Santin's long-term result is removed for further analysis. To demonstrate the latitudinal dependency, the linear interpolation is performed on the T_i trends of ISRs to get the values at the altitude of AO-ISR. And then, the variations of T_i trends are presented in Figure 11 as a function of geographic latitude

21699402, 2023, 2, Downloaded from https://agupubs.onlinelibrary.wiley.com/doi/10.1029/2022JA031049, Wiley Online Library on [02/04/2023]. See the Terms and Conditions (https://onlinelibrary.wiley.com/terms-and-conditions) on Wiley Online Library for rules of use; OA articles are governed by the applicable Creative Commons License

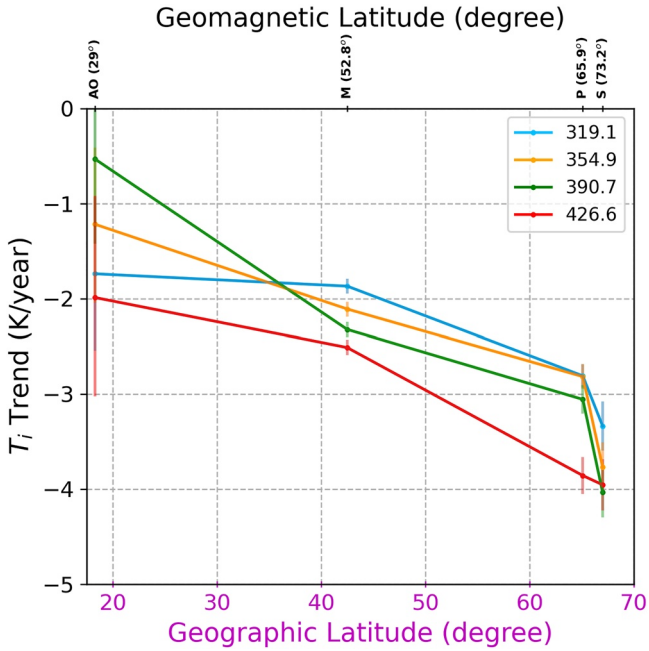

Figure 11. Variation of T_i trends as a function of geographic latitude at different altitudes (blue - 319.1 km, orange - 354.9 km, green - 390.7 km, and red - 426.6 km).

(pink) at different altitudes (blue - 319.1 km, orange - 354.9 km, green - 390.7 km, and red - 426.6 km). The geomagnetic latitudes of ISRs are given on the *x*-axis at the top. In Figure 11, the negative T_i trends are increasing as a function of geographic latitude/poleward. Cooling trends of ISRs are falling in place to support latitudinal dependency even though only four points (ISRs) are presented. Thus, coincidence is unlikely.

Above 500 km, AO-ISR observed rapid cooling trends as a function of altitude during the daytime, whereas nighttime cooling trends are almost steady at around −2 K/year in those comparable altitudes. Unfortunately, other ISRs are limited to 475 km, and the trends of AO-ISR estimation show enhanced values of 95% confidence intervals at high altitudes. Over Arecibo, the nighttime trends are mostly smaller than the daytime trends.

The trend profile of AO-ISR has different features than any other ISRs, especially within the altitude range of ∼150–400 km. Notably, there is no simple altitude dependency found over Arecibo. For that reason, we compare the trends of AO-ISR with those of the WACCM-X model. WACCM-X model trends are computed for the locations of AO-ISR and Millstone Hill-ISR. WACCM-X model for Millstone Hill is chosen since the cooling trends over there increases with altitude monotonically above ∼170 km in which altitudes the trends of AO-ISR differ. In this altitude range, cooling trends of AO-ISR increase with altitude up to ∼265 km (−2.1 K/year) during the daytime, and it decreases with altitude above ∼265 km (∼158 km during the night) till ∼400 km. This feature is evident in the WACCM-X model over Arecibo, especially for daytime; the cooling trends from the WACCM-X model increase with altitude from ∼122 km (−0.25 K/year) to ∼265 km (−0.9 K/year) and it decreases with altitude from ∼265 km (−0.9 K/year) to ∼400 km (−0.53 K/year). In this altitude range, the WACCM-X model over Millstone Hill shows a similar altitude profile of cooling trends even with closely similar cooling trends below ∼300 km. Above ∼300 km till ∼400 km, stronger cooling trends are found over Arecibo than Millstone Hill, which is opposite to the trends from ISRs over those locations. Furthermore, this is the altitude range where the nighttime trends of AO-ISR are closely comparable with the WACCM-X model. In remaining altitudes, the cooling trends are mostly stronger than those in the WACCM-X model.

4. Summary and Discussion

We have studied the long-term trends in ion temperature using incoherent scatter data from the Arecibo Observatory from 1985 to 2019. We have compared the trends to those from other ISR sites and to the WACCM-X model. The following is a list of our results:

1. Ion temperatures (T_i) are found to be highly sensitive to solar activity (represented by the $F_{10.7}$ flux) during both day and night, but much less so to the A_p index.
2. Removal of the quadratic term of $F_{10.7}$ from the T_i model causes enhanced and reduced cooling relatively depending on the time of the day and altitudes. Enhanced cooling resulted from removing this term above the altitude of ∼400 km during the day, whereas it occurs almost in all altitudes during the night. The reduced cooling is found to occur below the altitude of ∼400 km during the day.
3. Removal of A_p index resulted in cooling trends opposite to those resulting from the removal of the quadratic term of $F_{10.7}$ from the T_i model.
4. The contributions of the quadratic term of $F_{10.7}$ and A_p index to the T_i trends are found to be significant over Arecibo. Hence, we use those terms in modeling T_i variations.
5. Generally over Arecibo, the trend (from ISR) magnitudes and the 95% confidence intervals on average increase with altitude in the altitudes above ∼400 km, and the trends decrease with altitude till ∼400 km from ∼250 (∼158) km during the day (night). Generally, stronger T_i cooling trends are found in the daytime than nighttime, and those differences are within ∼1 K/year in altitudes below ∼500 km.
6. Interestingly, there is no overestimation of AO-ISR T_i trends below 200 km and above 400 km altitudes, as pointed out by Perrone and Mikhailov (2017), due to the sensitivity of the ISR observations to the T_i/m^+. Since no warming trends are estimated below 200 km or/and above 400 km altitudes.

21699402, 2023, 2, Downloaded from https://agupubs.onlinelibrary.wiley.com/doi/10.1029/2022JA031049, Wiley Online Library on [02/04/2023]. See the Terms and Conditions (https://onlinelibrary.wiley.com/terms-and-conditions) on Wiley Online Library for rules of use; OA articles are governed by the applicable Creative Commons License

21699402, 2023, 2, Downloaded from https://agupubs.onlinelibrary.wiley.com/doi/10.1029/2022JA031049, Wiley Online Library on [02/04/2023]. See the Terms and Conditions (https://onlinelibrary.wiley.com/terms-and-conditions) on Wiley Online Library for rules of use; OA articles are governed by the applicable Creative Commons License

7. Cooling trends from ISR and WACCM-X model over AO show a similar decrease with altitude from ~250 to ~400 km. Mostly, AO-ISR cooling trends are stronger than the WACCM-X model during the day, whereas nighttime ISR trends are very closely comparable with the WACCM-X model from ~300 till ~400 km. At these altitudes of ~300 to ~400 km, the cooling trend over Millstone Hill from the WACCM-X model decreases with altitude whereas the ISR cooling trend increases with altitude which is opposite to Arecibo trends.
8. In the comparison of ISRs trends, the AO-ISR also falls in place to support magnetic latitude dependency as increasing cooling trends with increasing magnetic latitudes in the altitudes of ~325–450 km except for St. Santin.

Over Arecibo, comparison of T_i trends during day and night reveals that stronger cooling is observed mostly during the daytime than at nighttime. A similar value of trends are also observed in both times at few altitudes over Arecibo. Similarly, a significant difference was observed between day and night over Millstone Hill, Sondrestrom, and Chatanika/Poker Flat (Zhang & Holt, 2013; Zhang et al., 2016). Stronger cooling occurs during the day than at night at all the altitudes over Sondrestrom and Arecibo. It was the other way around over Chatanika/Poker Flat, such as stronger cooling during the night than at day. Over Millstone Hill, stronger cooling was observed during the day than at night up to 450 km. Above 450 km, the relationship flips as stronger cooling was observed during the night than at day.

Most of the linear T_i trends from the ISRs are cooling trends. Generally, above the altitudes of 200 km, cooling trends are observed at all latitudes (Donaldson et al., 2010; Zhang & Holt, 2013; Zhang et al., 2016, 2011) except high-latitude-station Tromso, where warming was observed above 400 km (Ogawa et al., 2014). From 200 to 400 km altitude, the global mean T_n trend was calculated to be 4–6 K/decade using the neutral density trend (Akmaev, 2012). This means 0.4–0.6 K/year, which is smaller than Arecibo's T_i trends (−1.58 K/year) and comparable to or larger than Millstone Hill's T_i trends of −0.35 K/year as a gross average in the highly dynamical altitude region (Zhang & Holt, 2013). At the altitude of 225–325 km, T_i is approximately equal to T_n. The estimated average T_i trend over Millstone Hill and Arecibo is −0.35 and −1.92 K/year, respectively. During the daytime, stronger cooling exists over Arecibo than Millstone Hill at these altitudes.

At the altitude of 200–250 km, stronger cooling occurs over Arecibo than any other ISRs, as shown in Figure 10. Whereas Arecibo has weaker cooling trends than any other ISR facilities at the altitude range of 350–470 km, it is the altitude range where clear latitude dependency exists. The latitudinal dependency is obvious among the ISR facilities except for St. Santin. Even though the T_i data are from different periods among ISRs (Sondrestrom, Poker Flat, Millstone Hill, and Arecibo), the same method is used to obtain the trends for comparison (Zhang & Holt, 2013, 2016). From high-mid latitude, the strength of cooling trends is decreasing. Even though the latitudinal dependency of T_i trends exists in that altitude range, each location appears to have unique features.

Over Arecibo, trends from AO-ISR decrease with altitude till ~400 km altitude from ~250 (~158) km during the day (night). Daytime trends of AO-ISR increase with altitude from ~158 to ~250 km. This feature of the altitude profile, especially daytime trends, matches with Tromso trend profile, but there is a difference in altitudes and magnitudes. Within the altitude range of 250–400 km, cooling trends of Tromso (Arecibo) increase with altitude till ~330 (250) km from ~260 (175) km and decrease with altitude after that altitude of ~330 (250) km. Above 400 km, warming trends are observed over Tromso, whereas cooling trends are observed over Arecibo (Ogawa et al., 2014). This warming trend above 400 km altitude over Tromso was pointed out by Perrone and Mikhailov (2017) to be overestimated from the real T_i. They also found the overestimation of T_i trends in F_1 region heights over various ISR locations. In the F_1 region below 200 km, the negative trends should result in T_i trends over various ISR locations due to the negative trend in mean ion mass. Interestingly, there is no overestimation of T_i trends from the AO-ISR below 200 km and above 400 km altitudes since there are no positive trends in those altitude ranges, as pointed out by Perrone and Mikhailov (2017), due to the sensitivity of the ISR observations to the T_i/m^+.

Cooling trends from ISR and WACCM-X model over AO show a similar feature of decrease with altitude from ~250 till ~400 km (covering five altitude bins). Mostly, AO-ISR cooling trends are stronger than the WACCM-X model during the day, whereas nighttime ISR trends are very much closely comparable with the WACCM-X model from ~320 till ~400 km. At these altitudes of ~320–400 km, a comparison of cooling trends from the WACCM-X model and ISRs over Arecibo with Millstone Hill show distinct features over both locations. Rather, Millstone Hill ISR observed increasing cooling trends as a function of altitude, which is found in the overall

21699402, 2023, 2, Downloaded from https://agupubs.onlinelibrary.wiley.com/doi/10.1029/2022JA031049, Wiley Online Library on [02/04/2023]. See the Terms and Conditions (https://onlinelibrary.wiley.com/terms-and-conditions) on Wiley Online Library for rules of use; OA articles are governed by the applicable Creative Commons License

trends of Saint Santin, and Chatanika/Poker Flat. Around the altitude of 570 km, the warming trend is estimated by the WACCM-X model, whereas ISRs estimate cooling trends.

In WACCM-X model simulations, the thermosphere-ionosphere trends are driven by the trends of the two drivers, such as GHGs concentrations and the Earth's magnetic field (Cnossen, 2020a; Qian et al., 2021). Even though the WACCM-X model simulations were different between Cnossen (2020a) and Qian et al. (2021), their simulations include the increase in GHG concentrations and the changes in Earth's magnetic field to drive the long-term change in the upper atmosphere. Therefore, we assume that the findings of WACCM-Xs are the same since the drivers of long-term change are the same. Over Arecibo at the altitudes of ∼320–400 km at night, cooling trends might be derived by those two drivers in comparable contributions based on the conclusions of Qian et al. (2021) since ISR trends are very closely comparable to the WACCM-X model, as shown in Figure 10. During the day, those two comparable drivers might be contributing to cooling at the altitude of ∼391 km, and the dominant driver of GHG might be cooling the ionosphere at ∼175 km. Except for those corresponding altitude ranges during night and day in AO-ISR measurements, overall altitudes have stronger cooling trends than model simulations. Over Millstone Hill above the altitude of 220 km, cooling trends are stronger in ISR measurements than in the WACCM-X model. These discrepancies between the WACCM-X model and ISR data sets were also reported by Qian et al. (2021).

Stronger cooling trends in ISRs than the WACCM-X model suggest that a large part of the cooling has a cause other than the contributions from the increasing GHG concentrations and magnetic field variations represented by the WACCM-X model. This significant part of enhanced cooling might be possible by the contributions from the unaccounted magnitude of these two drivers (if any), other drivers, or a combination of both. Further studies are needed to understand this enhanced cooling by removing the contributions of increasing GHG concentrations and magnetic field variations from the T_i model. Notably, AO-ISR T_i trends fall in place to support the latitudinal dependency, but only four ISR sites are used. To explore the variations of long-term trends over latitude and longitude, further studies may be conducted using the measurements of electron density from (Global Positioning System - Radio Occultation) GPS-RO over various locations.

Data Availability Statement

Solar flux F10.7, geomagnetic activity Ap index, and WACCM-X version 2.0 model data are available at https://lasp.colorado.edu/lisird/data/penticton_radio_flux/, http://wdc.kugi.kyoto-u.ac.jp/kp/index.html, and https://catalogue.ceda.ac.uk/uuid/dc91f5e39ae34fd883af81dfdbaf659c, respectively. ISR data are available at the madrigal (http://openmadrigal.org) website.

Acknowledgments
Authors gratefully thank the AO technical staff for their support in carrying out the ISR observations reported here and also thank the people who do the analysis and maintain the madrigal database at AO. The Arecibo Observatory is operated by the University of Central Florida under a cooperative agreement with the National Science Foundation (AST-1744119) and in alliance with Yang Enterprises and Ana G. Méndez-Universidad Metropolitana. Research at MIT Haystack Observatory is supported in part by NSF Geospace Facility grant AGS-1952737 and NASA LWS program 80NSSC21K1315. The author (D.S.) would like to thank his colleagues Dr. Sravani Vaddi and Dr. Alison Smith for their help in manuscript reading and fruitful discussion. The authors would like to thank one of the anonymous reviewers for their suggestions.

References

Akmaev, R. A. (2012). On estimation and attribution of long-term temperature trends in the thermosphere. *Journal of Geophysical Research*, *117*, A09321. https://doi.org/10.1029/2012JA018058

Akmaev, R. A., & Fomichev, V. I. (1998). Cooling of the mesosphere and lower thermosphere due to doubling of CO_2. *Annales Geophysicae*, *16*, 1501–1512. https://doi.org/10.1007/s00585-998-1501-z

Bremer, J. (1992). Ionospheric trends in mid-latitudes as a possible indicator of the atmospheric greenhouse effect. *Journal of Atmospheric and Terrestrial Physics*, *54*, 1505–1511. https://doi.org/10.1016/0021-9169(92)90157-G

Brum, C. G. M., Rodrigues, F. S., dos Santos, P. T., Matta, A. C., Aponte, N., Gonzalez, S. A., et al. (2011). A modeling study of f_0f_2 and h_mf_2 parameters measured by the Arecibo incoherent scatter radar and comparison with IRI model predictions for solar cycles 21–23. *Journal of Geophysical Research*, *116*, A03324. https://doi.org/10.1029/2010JA015727

Brum, C. G. M., Tepley, C. A., Fentzke, J. T., Robles, E., dos Santos, P. T., & Gonzalez, S. A. (2012). Long-term changes in the thermospheric neutral winds over Arecibo: Climatology based on over three decades of Fabry-Perot observations. *Journal of Geophysical Research*, *117*, A00H14. https://doi.org/10.1029/2011JA016458

Cai, Y., Yue, X., Wang, W., Zhang, S., Liu, L., Liu, H., & Wan, W. (2019). Long-term trend of topside ionospheric electron density derived from DMSP data during 1995–2017. *Journal of Geophysical Research: Space Physics*, *124*, 10708–10727. https://doi.org/10.1029/2019JA027522

Clilverd, M. A., Ulich, T., & Jarvis, M. J. (2003). Residual solar cycle influence on trends in ionospheric F2-layer peak height. *Journal of Geophysical Research*, *108*(A12), 1450. https://doi.org/10.1029/2003JA009838

Cnossen, I. (2014). The importance of geomagnetic field changes versus rising CO_2 levels for long-term change in the upper atmosphere. *Journal of Space Weather and Space Climate*, *4*, A18. https://doi.org/10.1051/swsc/2014016

Cnossen, I. (2020a). Analysis and attribution of climate change in the upper atmosphere from 1950 to 2015 simulated by WACCM-X. *Journal of Geophysical Research: Space Physics*, *125*, e2020JA028623. https://doi.org/10.1029/2020JA028623

Cnossen, I. (2020b). *Monthly mean climate data from a transient simulation with the Whole Atmosphere Community Climate Model eXtension (WACCM-X) from 1950 to 2015*. Centre for Environmental Data Analysis. https://doi.org/10.5285/dc91f5e39ae34fd883af81dfdbaf659c

Cnossen, I. (2022a). A realistic projection of climate change in the upper atmosphere into the 21st century. *Geophysical Research Letters*, *49*, e2022GL100693. https://doi.org/10.1029/2022GL100693

Cnossen, I. (2022b). *Monthly mean climate data from a transient simulation with the Whole Atmosphere Community Climate Model eXtension (WACCM-X) from 2015 to 2070*. NERC EDS Centre for Environmental Data Analysis. https://doi.org/10.5285/45283390b97c4a27861d74b3d915b0bd

Donaldson, J. K., Wellman, T. J., & Oliver, W. L. (2010). Long-term change in thermospheric temperature above Saint Santin. *Journal of Geophysical Research*, *115*, A11305. https://doi.org/10.1029/2010JA015346

Emmert, J. T. (2015). Altitude and solar activity dependence of 1967–2005 thermospheric density trends derived from orbital drag. *Journal of Geophysical Research: Space Physics*, *120*, 2940–2950. https://doi.org/10.1002/2015JA021047

Emmert, J. T., Lean, J. L., & Picone, J. M. (2010). Record-low thermospheric density during the 2008 solar minimum. *Geophysical Research Letters*, *37*, L12102. https://doi.org/10.1029/2010GL043671

Emmert, J. T., Picone, J. M., Lean, J. L., & Knowles, S. H. (2004). Global change in the thermosphere: Compelling evidence of a secular decrease in density. *Journal of Geophysical Research*, *109*, A02301. https://doi.org/10.1029/2003JA010176

Emmert, J. T., Picone, J. M., & Meier, R. R. (2008). Thermospheric global average density trends. *Geophysical Research Letters*, *35*, L05101. https://doi.org/10.1029/2007GL032809

Holt, J., & Zhang, S. (2008). Long-term temperature trends in the ionosphere above Millstone Hill. *Geophysical Research Letters*, *35*, L05813. https://doi.org/10.1029/2007GL031148

Keating, G. M., Tolson, R. H., & Bradford, M. S. (2000). Evidence of long-term global decline in the Earth's thermospheric densities apparently related to anthropogenic effects. *Geophysical Research Letters*, *27*, 1523–1526. https://doi.org/10.1029/2000GL003771

Laštovička, J. (2015). Comment on "long-term trends in thermospheric neutral temperatures and density above Millstone Hill" by W. L. Oliver et al. *Journal of Geophysical Research: Space Physics*, *120*, 2347–2349. https://doi.org/10.1002/2014JA020864

Laštovička, J. (2021). Long-term trends in the upper atmosphere. *Geophysical Monograph Series* Chapter 17. https://doi.org/10.1002/9781119815631.ch17

Laštovička, J., Akmaev, R. A., Beig, G., Bremer, J., & Emmert, J. T. (2006). Global change in the upper atmosphere. *Science*, *314*(5803), 1253–1254. https://doi.org/10.1126/science.1135134

Liu, H.-L., Bardeen, C. G., Foster, B. T., Lauritzen, P., Liu, J., Lu, G., et al. (2018). Development and validation of the Whole Atmosphere Community Climate Model with Thermosphere and Ionosphere eXtension (WACCM-X 2.0). *Journal of Advances in Modeling Earth Systems*, *10*(2), 381–402. https://doi.org/10.1002/2017MS001232

Liu, H.-L., Tao, C., Jin, H., & Abe, T. (2021). Geomagnetic activity effects on CO_2-driven trend in the thermosphere and ionosphere: Ideal model experiments with Gaia. *Journal of Geophysical Research: Space Physics*, *126*, e2020JA028607. https://doi.org/10.1029/2020JA028607

Mikhailov, A. V. (2006). Ionospheric long-term trends: Can the geomagnetic control and the greenhouse hypotheses be reconciled? *Annales Geophysicae*, *24*, 2533–2541. https://doi.org/10.5194/angeo-24-2533-2006

Ogawa, Y., Motoba, T., Buchert, S. C., Häggström, I., & Nozawa, S. (2014). Upper atmosphere cooling over the past 33 years. *Geophysical Research Letters*, *41*, 5629–5635. https://doi.org/10.1002/2014GL060591

Oliver, W. L., Holt, J. M., Zhang, S.-R., & Goncharenko, L. P. (2014). Long-term trends in thermospheric neutral temperature and density above Millstone Hill. *Journal of Geophysical Research: Space Physics*, *119*, 7940–7946. https://doi.org/10.1002/2014JA020311

Oliver, W. L., Holt, J. M., Zhang, S.-R., & Goncharenko, L. P. (2015). Reply to comment by Jan Lastovička on "long-term trends in thermospheric neutral temperature and density above Millstone Hill". *Journal of Geophysical Research: Space Physics*, *120*, 2350–2352. https://doi.org/10.1002/2014JA020967

Oliver, W. L., Zhang, S.-R., & Goncharenko, L. P. (2013). Is thermospheric global cooling caused by gravity waves? *Journal of Geophysical Research: Space Physics*, *118*, 3898–3908. https://doi.org/10.1002/jgra.50370

Perrone, L., & Mikhailov, A. V. (2017). Long-term variations of exospheric temperature inferred from f_0f_1 observations: A comparison to ISR t_i trend estimates. *Journal of Geophysical Research: Space Physics*, *122*(5803), 8883–8892. https://doi.org/10.1002/2017JA024193

Qian, L., Laštovička, J., Roble, R. G., & Solomon, S. C. (2011). Progress in observations and simulations of global change in the upper atmosphere. *Journal of Geophysical Research*, *116*, A00H03. https://doi.org/10.1029/2010JA016317

Qian, L., McInerney, J. M., Solomon, S. S., Liu, H., & Burns, A. G. (2021). Climate changes in the upper atmosphere: Contributions by the changing greenhouse gas concentrations and Earth's magnetic field from the 1960s to 2010s. *Journal of Geophysical Research: Space Physics*, *126*, e2020JA029067. https://doi.org/10.1029/2020JA029067

Rishbeth, H. (1990). A greenhouse effect in the ionosphere. *Planetary and Space Science*, *38*, 945–948. https://doi.org/10.1016/0032-0633(90)90061-T

Roble, R. G., & Dickinson, R. E. (1989). How will changes in carbon dioxide and methane modify the mean structure of the mesosphere and thermosphere? *Geophysical Research Letters*, *16*, 1441–1444. https://doi.org/10.1029/GL016i012p01441

Santos, P. T., Brum, C. G. M., Tepley, C. A., Aponte, N., González, S. A., & Robles, E. (2011). Using incoherent scatter radar to investigate the neutral wind long-term trend over Arecibo. *Journal of Geophysical Research*, *116*, A00H13. https://doi.org/10.1029/2011JA016514

Yue, X., Hu, L., Wei, Y., Wan, W., & Ning, B. (2018). Ionospheric trend over Wuhan during 1947–2017: Comparison between simulation and observation. *Journal of Geophysical Research: Space Physics*, *123*(2), 1396–1409. https://doi.org/10.1002/2017JA024675

Zhang, S.-R., & Holt, J. M. (2013). Long-term ionospheric cooling: Dependency on local time, season, solar activity, and geomagnetic activity. *Journal of Geophysical Research: Space Physics*, *118*, 3719–3730. https://doi.org/10.1002/jgra.50306

Zhang, S.-R., Holt, J. M., Erickson, P. J., Goncharenko, L. P., Nicolls, M. J., McCready, M., & Kelly, J. (2016). Ionospheric ion temperature climate and upper atmospheric long-term cooling. *Journal of Geophysical Research: Space Physics*, *121*, 8951–8968. https://doi.org/10.1002/2016JA022971

Zhang, S.-R., Holt, J. M., & Kurdzo, J. (2011). Millstone Hill ISR observations of upper atmospheric long-term changes: Height dependency. *Journal of Geophysical Research*, *116*, A00H05. https://doi.org/10.1029/2010JA016414

21699402, 2023, 2, Downloaded from https://agupubs.onlinelibrary.wiley.com/doi/10.1029/2022JA031049, Wiley Online Library on [02/04/2023]. See the Terms and Conditions (https://onlinelibrary.wiley.com/terms-and-conditions) on Wiley Online Library for rules of use; OA articles are governed by the applicable Creative Commons License